Thermal Transformation of Metal Oxide Nanoparticles into Nanocrystalline Metal Nitrides Using Cyanamide and Urea as Nitrogen Source

Jelena Buha,[†] Igor Djerdj,[†,‡] Markus Antonietti,[†] and Markus Niederberger*[,§]

Colloid Chemistry, Max Planck Institute of Colloids and Interfaces, Research Campus Golm, 14424 Potsdam, Germany, Department of Physics, Faculty of Science, University of Zagreb, Bijenička 32, P.O. Box 331, 10002 Zagreb, Croatia, and Department of Materials, Swiss Federal Institute of Technology (ETH) Zürich, Wolfgang-Pauli-Strasse 10, 8093 Zürich, Switzerland

Received January 19, 2007. Revised Manuscript Received April 20, 2007

Preformed metal oxide nanoparticles with varying crystallinity and different particle sizes and shapes can thermally be transformed into nanocrystalline metal nitrides in the presence of cyanamide or urea as nitrogen sources. In the case of anatase nanoparticles with crystallite sizes of 5, 10, and 20 nm, respectively, only the 5 nm sized TiO_2 transformed completely into TiN. According to powder X-ray diffraction (XRD) and transmission electron microscopy measurements (TEM), the TiN particles are rather uniform in size and shape with a crystallite size of 3−5 nm, depending on the nitrogen source. In contrast to titania, vanadium oxide nanoparticles of much larger sizes and with different shapes reacted to nanocrystalline VN. However, the morphological features of the precursor particles are not transcribed into the final metal nitrides with an average crystallite size of 15 nm. Crystallinity plays a role too, as only amorphous tantalum oxide could be converted into nanocrystalline TaN. Furthermore, aluminum oxide γ-Al_2O_3, gallium oxide γ-Ga_2O_3, and niobium oxide nanoparticles formed AlN, GaN, and NbN, respectively, whereas HfO_2 transformed into a hafnium oxide nitride compound. With the exception of GaN and TaN, all other metal nitrides contain amorphous carbon as byproduct. However, by adjusting the metal oxide-to-nitrogen source ratio, the carbon content can be minimized.

Introduction

Metal nitrides are a class of functional materials with increasing importance, complementing metal oxides in many applications. However, metal oxides outnumber nitrides by orders of magnitude, mainly due to the thermodynamic difficulties in making and breaking the nitrogen triple bond.[1] Similar to metal oxides, metal nitrides are characterized by an intriguing crystal chemistry, which leads to unique chemical and physical properties.[2−5] As a result, metal nitrides found diverse applications ranging from refractory ceramics[6,7] (AlN, TaN, TiN, ...) and wear-resistant coatings (TiN, ZrN, CrN, (Ti,Al)N, Zr_3N_4)[8−10] to semiconductor devices for optoelectronics (GaN, InN).[11,12]

The size- and shape-dependent physical properties of semiconductors as well as the high surface-to-volume ratio are the major driving forces behind the synthesis of nanomaterials.[13−15] This is also true for metal nitrides, and in the past few years, great efforts have been made to achieve them as nanoparticulate materials. The reported synthesis procedures comprise a wide range of techniques, including hydrazide sol−gel synthesis,[16] solvothermal routes,[17−23] nitridation or ammonolysis of molecular precursors,[24−28]

* To whom correspondence should be addressed. E-mail: markus.niederberger@mat.ethz.ch.
† Max Planck Institute of Colloids and Interfaces.
‡ University of Zagreb.
§ Swiss Federal Institute of Technology.

(1) Gregory, D. H. *J. Chem. Soc., Dalton Trans.* **1999**, 259−270.
(2) Breese, N. E. Crystal Chemistry of Inorganic Nitrides. In *Structure and Bonding*; Springer-Verlag: Berlin, 1992.
(3) Niewa, R.; DiSalvo, F. J. *Chem. Mater.* **1998**, *10*, 2733−2752.
(4) Miao, M. S.; Lukashev, P.; Herwadkar, A.; Lambrecht, W. R. L. *Phys. Status Solidi C* **2005**, *2*, 2516−2519.
(5) Zheng, W. T.; Sun, C. Q. *Prog. Solid State Chem.* **2006**, *34*, 1−20.
(6) Dahotre, N. B.; Kadolkar, P.; Shah, S. *Surf. Interface Anal.* **2001**, *31*, 659−672.
(7) Schlesser, R.; Dalmau, R.; Zhuang, D.; Collazo, R.; Sitar, Z. *J. Cryst. Growth* **2005**, *281*, 75−80.
(8) Milosev, I.; Strehblow, H.-H.; Navinsek, B. *Solid State Ionics* **1997**, *303*, 245−254.
(9) PalDey, S.; Deevi, S. C. *Mater. Sci. Eng., B* **2003**, *361*, 1−8.
(10) Zerr, A.; Riedel, R.; Sekine, T.; Lowther, J. E.; Ching, W.-Y.; Tanaka, I. *Adv. Mater.* **2006**, *18*, 2933−2948.
(11) Ambacher, O. *J. Phys. D: Appl. Phys.* **1998**, *31*, 2653−2710.
(12) Bhuiyan, A. G.; Hashimoto, A.; Yamamoto, A. *J. Appl. Phys.* **2003**, *94*, 2779−2808.
(13) Henglein, A. *Chem. Rev.* **1989**, *89*, 1861−1873.
(14) Steigerwald, M. L.; Brus, L. E. *Acc. Chem. Res.* **1990**, *23*, 183−188.
(15) Alivisatos, A. P. *J. Phys. Chem.* **1996**, *100*, 13226−13239.
(16) Kim, I.-S.; Kumta, P. N. *J. Mater. Chem.* **2003**, *13*, 2028−2035.
(17) Grocholl, L.; Wang, J.; Gillan, E. G. *Chem. Mater.* **2001**, *13*, 4290−4296.
(18) Xiao, J.; Xie, Y.; Tang, R.; Luo, W. *Inorg. Chem.* **2003**, *42*, 107−111.
(19) Desmoulins-Krawiec, S.; Aymonier, C.; Loppinet-Serani, A.; Weill, F.; Gorsse, S.; Etourneau, J.; Cansell, F. *J. Mater. Chem.* **2004**, *14*, 228−232.
(20) Xiong, Y. J.; Xie, Y.; Li, Z. Q.; Li, X. O.; Zhang, R. *New J. Chem.* **2004**, *28*, 214−217.
(21) Sardar, K.; Deepak, F. L.; Govindaraj, A.; Seikh, M. M.; Rao, C. N. R. *Small* **2005**, *1*, 91−94.
(22) Wu, C. Z.; Li, T. W.; Lei, L. Y.; Hu, S. Q.; Liu, Y.; Xie, Y. *New J. Chem.* **2005**, *29*, 1610−1615.
(23) Choi, J.; Gillan, E. G. *J. Mater. Chem.* **2006**, *16*, 3774−3784.
(24) Barry, S. T.; Richeson, D. S. *Chem. Mater.* **1994**, *6*, 2220−2221.
(25) Kaskel, S.; Schlichte, K.; Chaplais, G.; Khanna, M. *J. Mater. Chem.* **2003**, *13*, 1496−1499.
(26) Schwenzer, B.; Meier, C.; Masala, O.; Seshadri, R.; DenBaars, S. P.; Mishra, U. K. *J. Mater. Chem.* **2005**, *15*, 1891−1895.

10.1021/cm0701759 CCC: $37.00
Published on Web 06/09/2007

various metathesis routes,[29−31] and chemical transformation of molecular precursors in solution.[32,33] In some cases, control over crystal growth was achieved by performing the reaction in the nanoconfinement of mesoporous materials like SBA-15[34,35] or mpg-C_3N_4.[36]

In spite of all these reports, the number and variety of nanocrystalline metal nitrides is still rather restricted, especially when compared to metal oxide nanoparticles. Therefore, it is obvious to use preformed metal oxides as precursors for the preparation of metal nitrides. The first results in this direction, although starting from metal halides, were published more than 10 years ago by Kawaguchi et al.[37] The reaction of $AlCl_3$ with $[(C_3N_3)_2(NH)_3]_n$ at 1000 °C yielded AlN. The direct transformation of metal oxides is possible in the carbothermal reduction process.[38−43] In one approach, the metal oxides were reacted with carbon under nitrogen or ammonia.[38−42] The other route involved the reaction of Ga_2O_3 with $C_3N_{3.69}$ at 650 °C in an evacuated ampule.[43] The GaN nanocrystallites were in the size range of 30−50 nm. Recently, the same authors simplified this reaction approach by exchanging $C_3N_{3.69}$ against melamine as nitrogen source, enabling the transformation of various bulk metal oxides like Ga_2O_3, Cr_2O_3, Al_2O_3, TiO_2, V_2O_5, Nb_2O_5, and Ta_2O_5 into the respective metal nitrides.[44] Depending on the precursor oxide, the reaction temperatures ranged from 650 to 1200 °C, and the metal nitrides had crystallite sizes of 20 to 100 nm. Other approaches based on the transformation of metal oxides into metal nitrides or metal oxynitrides include plasma nitridation,[45] ammonolysis,[46−50] cyanonitridation using monomethylamine,[51] thermolysis under nitrogen,[52,53] or reaction with sodium amide.[54]

In this article, we report the thermal transformation of various metal oxide nanoparticles into nanocrystalline metal nitrides. Nanosized oxides of titanium, aluminum, gallium, vanadium, niobium, hafnium, and tantalum were used as precursor materials and cyanamide or urea as nitrogen source. The oxidic nanopowders were transformed into the metal nitrides upon heating them together in a crucible at 800 °C under a nitrogen atmosphere. For the first time, a detailed study is presented on the influence of the structural and morphological properties of the starting nanomaterials on the characteristics of the final metal nitrides. To correlate the particle size and shape of the starting metal oxides with the final nitrides, we chose the following systems as instructive examples: (i) nearly spherical anatase nanoparticles with crystallite sizes of about 5, 10, and 20 nm, respectively; (ii) two types of vanadium oxide nanoparticles, isotropic V_2O_3 particles in the size range of 20−50 nm and anisotropic VO_x nanorods 20−50 nm wide and 150−250 nm long; (iii) amorphous and crystalline tantalum oxide nanoparticles. Furthermore, the wide applicability of the synthesis approach was proven by the transformation of γ-Al_2O_3 nanocrystals to AlN, γ-Ga_2O_3 nanoparticles to GaN, Nb_2O_5 to $Nb_4N_{3.92}$, and HfO_2 to Hf_2ON_2. The nitrogen sources were chosen according to literature, where the successful use of urea for the preparation of several binary metal nitrides[55,56] and cyanamide for the synthesis of melem, a precursor for graphitic carbon nitride,[57] and g-C_3N_4 nanoparticles in mesoporous silica[58,59] have recently been reported.

Experimental Section

Materials. Cyanamide (99%, Aldrich) and urea (puriss, Riedel-de-Haen) were used as received. The thermal transformation was performed in Nabertherm Multitherm N 7/H lab furnaces under a nitrogen gas flow (4.0, Praxair).

Synthesis. In a typical procedure, 100 mg of the oxidic nanopowders were mixed with 2 g of cyanamide or urea and reacted at 800 °C under a nitrogen atmosphere. In selected cases (see main text), the temperature was increased to 900 °C. The oxidic nanopowders were synthesized according to previously reported procedures. Five-nanometer-sized TiO_2 was obtained from $TiCl_4$ and benzyl alcohol;[60] 10 nm sized TiO_2 was obtained from titanium

(27) Jackson, A. W.; Shebanova, O.; Hector, A. L.; McMillan, P. F. *J. Solid State Chem.* **2006**, *179*, 1383−1393.
(28) Choi, D.; Blomgren, G. E.; Kumta, P. N. *Adv. Mater.* **2006**, *18*, 1178−1182.
(29) Wang, J. J.; Grocholl, L.; Gillan, E. G. *Nano Lett.* **2002**, *2*, 899−902.
(30) Chen, L. Y.; Gu, Y. L.; Shi, L.; Yang, Z. H.; Ma, J. H.; Qian, Y. T. *Solid State Commun.* **2004**, *132*, 343−346.
(31) Joshi, U. A.; Chung, S. H.; Lee, J. S. *J. Solid State Chem.* **2005**, *178*, 755−760.
(32) Micic, O. I.; Ahrenkiel, S. P.; Bertram, D.; Nozik, A. J. *Appl. Phys. Lett.* **1999**, *75*, 478−480.
(33) Pan, G. Q.; Kordesch, M. E.; Van Patten, P. G. *Chem. Mater.* **2006**, *18*, 5392−5394.
(34) Hsueh, H. S.; Yang, C. T.; Zink, J. I.; Huang, M. H. *J. Phys. Chem. B* **2005**, *109*, 4404−4409.
(35) Yang, C.-T.; Huang, M. H. *J. Phys. Chem. B* **2005**, *109*, 17842−17847.
(36) Fischer, A.; Antonietti, M.; Thomas, A. *Adv. Mater.* **2007**, *19*, 264−267.
(37) Kawaguchi, M.; Nozaki, K. *Chem. Mater.* **1995**, *7*, 257−264.
(38) White, G. V.; Mackenzie, K. J. D.; Johnston, J. H. *J. Mater. Sci.* **1992**, *27*, 4287−4293.
(39) White, G. V.; Mackenzie, K. J. D.; Brown, I. W. M.; Bowden, M. E.; Johnston, J. H. *J. Mater. Sci.* **1992**, *27*, 4294−4299.
(40) White, G. V.; Mackenzie, K. J. D.; Brown, I. W. M.; Johnston, J. H. *J. Mater. Sci.* **1992**, *27*, 4300−4304.
(41) Vaidhyanathan, B.; Rao, K. J. *Chem. Mater.* **1997**, *9*, 1196−1200.
(42) Sun, X. M.; Li, Y. *Angew. Chem., Int. Ed.* **2004**, *43*, 3827−3831.
(43) Zhao, H.; Lei, M.; Yang, X.; Jian, J.; Chen, X. *J. Am. Chem. Soc.* **2005**, *127*, 15722−15723.
(44) Zhao, H.; Lei, M.; Chen, X.; Tang, W. *J. Mater. Chem.* **2006**, *16*, 4407−4412.
(45) Houmes, J. D.; zur Loye, H. C. *Chem. Mater.* **1996**, *8*, 2551−2553.
(46) Schwenzer, B.; Loeffler, L.; Seshadri, R.; Keller, S.; Lange, F. F.; DenBaars, S. P.; Mishra, U. K. *J. Mater. Chem.* **2004**, *14*, 637−641.
(47) Schwenzer, B.; Hu, J.; Seshadri, R.; Keller, S.; DenBaars, S. P.; Mishra, U. K. *Chem. Mater.* **2004**, *16*, 5088−5095.
(48) Luo, S. D.; Zhou, W. Y.; Zhang, Z. X.; Liu, L. F.; Dou, X. Y.; Wang, J. X.; Zhao, X. W.; Liu, D. F.; Gao, Y.; Song, L.; Xiang, Y. J.; Zhou, J. J.; Xie, S. S. *Small* **2005**, *1*, 1004−1009.
(49) Henderson, S. J.; Hector, A. L. *J. Solid State Chem.* **2006**, *179*, 3518−3524.
(50) a) Chen, H.; Nambu, A.; Wen, W.; Graciani, J.; Zhong, Z.; Hanson, J. C.; Fujita, E.; Rodriguez, J. A. *J. Phys. Chem. C* **2007**, *111*, 1366−1372; b) Schwartz, V.; Oyama, S. T. *Chem. Mater.* **1997**, *9*, 3052−3059.
(51) Clement, F.; Bastians, P.; Grange, P. *Solid State Ionics* **1997**, 101−103, 171−174.
(52) Li, J.; Gao, L.; Sun, J.; Zhang, Q.; Guo, J.; Yan, D. *J. Am. Ceram. Soc.* **2001**, *84*, 3045−3047.
(53) Dezelah, C. L.; El-Kadri, O. M.; Heeg, M. J.; Winter, C. H. *J. Mater. Chem.* **2004**, *14*, 3167−3176.
(54) Huang, Y.; Gu, Y.; Zheng, M.; Xu, Z.; Zeng, W.; Liu, Y. *Mater. Lett.* **2007**, *61*, 1056−1059.
(55) Sardar, K.; Dan, M.; Schwenzer, B.; Rao, C. N. R. *J. Mater. Chem.* **2005**, *15*, 2175−2177.
(56) Gomathi, A.; Rao, C. N. R. *Mater. Res. Bull.* **2006**, *41*, 941−947.
(57) Jurgens, B.; Irran, E.; Senker, J.; Kroll, P.; Muller, H.; Schnick, W. *J. Am. Chem. Soc.* **2003**, *125*, 10288−10300.
(58) Groenewolt, M.; Antonietti, M. *Adv. Mater.* **2005**, *17*, 1789−1792.
(59) Goettmann, F.; Fischer, A.; Antonietti, M.; Thomas, A. *Angew. Chem., Int. Ed.* **2006**, *45*, 4467−4471.

isopropoxide and acetophenone and 20 nm sized TiO_2 was obtained from titanium isopropoxide and 2-butanone.[61] Ga_2O_3 was obtained from gallium acetylacetonate and either benzylamine, octylamine, or a mixture of both solvents,[62] aluminum oxide from aluminum acetylacetonate and benzyl amine,[63] vanadium oxide nanorods from vanadium oxotrichloride and benzyl alchohol,[64] and V_2O_3 from vanadium oxotriisopropoxide and benzyl alcohol.[65] Crystalline tantalum, hafnium, and niobium oxide were synthesized from the respective metal chlorides and benzyl alcohol at 220 °C, whereas the amorphous tantalum oxide was obtained from tantalum ethoxide and benzyl alcohol.[66] Detailed synthesis procedures for every metal nitride can be found in the Supporting Information.

Characterization. The X-ray powder diffraction (XRD) patterns were measured in reflection mode (Cu Kα radiation) on a Bruker D8 diffractometer equipped with a scintillation counter. The structural and microstructural parameters were extracted using Rietveld refinement as reported before.[67] For the transmission electron microscopy (TEM) investigations, the samples were dispersed in ethanol and a few drops were deposited onto a copper grid covered by an amorphous carbon film. To prevent agglomeration of nanoparticles, we set the copper grid in a Petri dish whose bottom was covered with filter paper. Either a Zeiss EM 912Ω instrument at an acceleration voltage of 120 kV or, for high-resolution, selected area electron diffraction (SAED), and energy-dispersive X-ray (EDX) analysis, a Philips CM200-FEG microscope 200 kV equipped with field emission gun (the coefficient of spherical aberration was C_s = 1.35 mm) were used. Elemental analyses were carried out on a Vario EL Elementar (Elementar Analysensysteme, Germany).

Results and Discussion

The thermal transformation of TiO_2 nanoparticles provides a good opportunity to investigate whether there is a direct correlation of the crystallite size of the starting oxidic material with the final metal nitride particles. To achieve this objective, we reacted nanopowders consisting of anatase nanoparticles with average crystallite sizes of about 5, 10, and 20 nm, respectively, with urea and cyanamide at 800 °C under a nitrogen atmosphere. In general, 100 mg of the oxidic nanopowders were mixed with a large stoichiometric excess of 2 g of cyanamide or urea in a ceramic crucible. According to powder X-ray diffraction (XRD), only the anatase nanoparticles of 5 nm were completely transformed into TiN. In the case of TiO_2 with larger crystallite sizes of 10 and 20 nm, both nitrogen sources resulted in products with anatase impurities; however, there was no formation of the thermodynamically stable rutile phase.

The large excess of cyanamide and urea leads to the problem that in addition to the metal nitride, a large amount of amorphous carbon is also produced. As a matter of fact, elemental analysis of the TiN samples obtained from 5 nm sized TiO_2 and cyanamide or urea showed a carbon content of about 20−25 wt %. This problem can be solved by adjusting the metal oxide-to-nitrogen source ratio. In the case of titanium, the best results, i.e., formation of titanium nitride without any oxidic residues, were achieved by reacting 100 mg of anatase nanopowder with a crystallite size of 5 nm

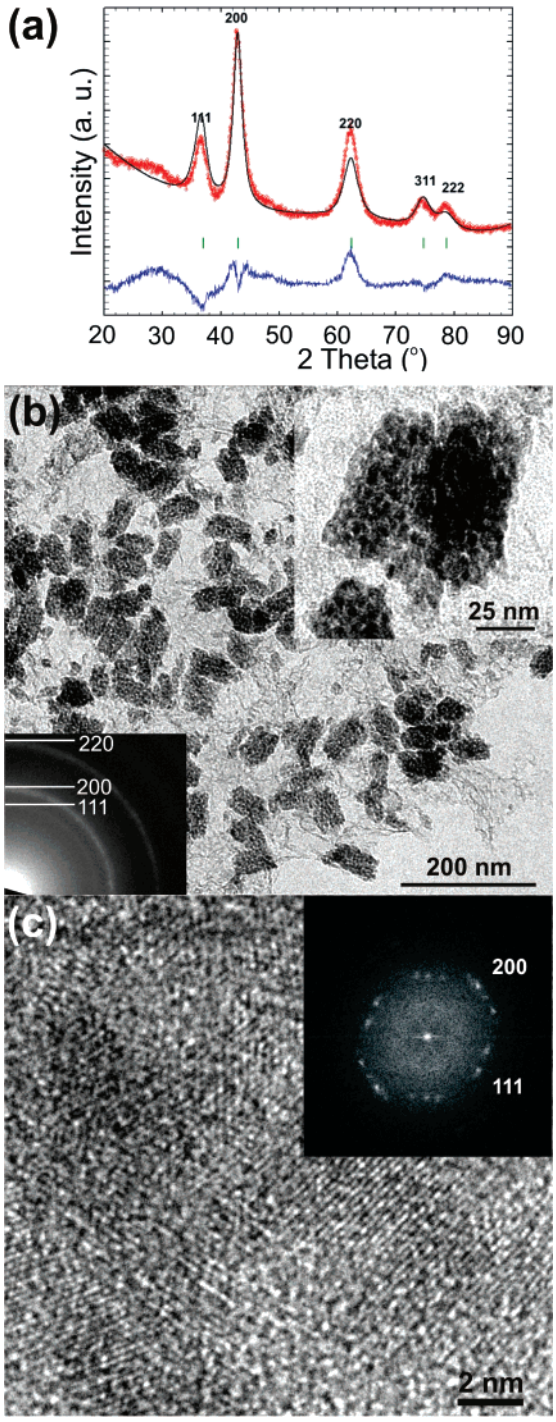

Figure 1. Titanium nitride nanoparticles obtained from 5 nm sized anatase nanoparticles and cyanamide. (a) Experimental XRD pattern (red), calculated pattern (black), difference curve (blue), and calculated values of the positions of the Bragg reflections (short green vertical bars). (b) TEM overview image: inset upper right, TEM image at higher magnification; inset lower left, corresponding SAED pattern. (c) HRTEM image of several nanoparticles together with the corresponding power spectrum as inset.

(60) Niederberger, M.; Bartl, M. H.; Stucky, G. D. *Chem. Mater.* **2002**, *14*, 4364−4370.
(61) Garnweitner, G.; Antonietti, M.; Niederberger, M. *Chem. Commun.* **2005**, 397−399.
(62) Pinna, N.; Garnweitner, G.; Antonietti, M.; Niederberger, M. *J. Am. Chem. Soc.* **2005**, *127*, 5608−5612.
(63) Zhou, S.; Antonietti, M.; Niederberger, M. *Small* **2007**, *3*, 763−767.
(64) Niederberger, M.; Bartl, M. H.; Stucky, G. D. *J. Am. Chem. Soc.* **2002**, *124*, 13642−13643.
(65) Pinna, N.; Antonietti, M.; Niederberger, M. *Colloids Surf., A* **2004**, *250*, 211−213.
(66) Pinna, N.; Garnweitner, G.; Antonietti, M.; Niederberger, M. *Adv. Mater.* **2004**, *16*, 2196−2200.
(67) Buha, J.; Djerdj, I.; Niederberger, M. *Cryst. Growth Des.* **2007**, *7*, 113−116.

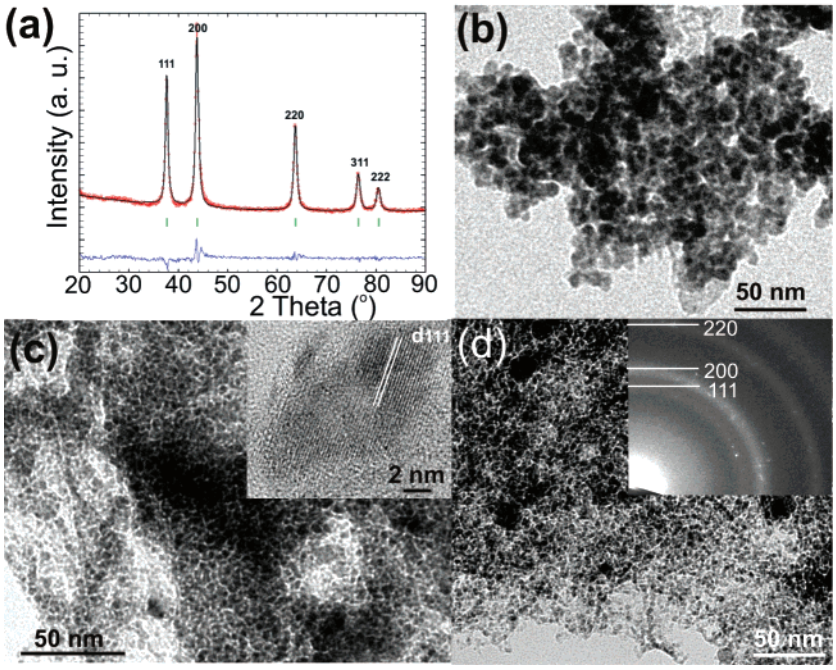

Figure 2. Vanadium nitride nanoparticles. (a) Representative experimental XRD pattern (red), calculated pattern (black), difference curve (blue), and calculated values of the positions of the Bragg reflections (short green vertical bars). (b) TEM overview image. Sample in (a) and (b) obtained from vanadium oxide nanorods and cyanamide. (c) TEM overview image with HRTEM micrograph with the lattice indexing as inset of VN from vanadium oxide nanorods and urea. (d) TEM overview image of VN from V_2O_3 and cyanamide with corresponding SAED pattern.

with 100.8 mg of cyanamide, yielding titanium nitride nanoparticles with a carbon content of about 2 wt %. Figure 1 gives an overview of the structural and morphological properties of the TiN nanoparticles obtained under these conditions. Figure 1a displays the experimental powder X-ray pattern together with the calculated pattern obtained from Rietveld refinement and the difference profile. The TiN nanoparticles are crystalline and the reflections can be indexed according to the cubic structure with the space group $Fm\bar{3}m$ (ICDD PDF 38-1420). There is no indication for the presence of any other crystalline phase like remaining oxides. The very broad peak, which appears at around 28°, is evidence of the presence of amorphous carbon as byproduct. The broad reflections point to small crystallite sizes. According to Rietveld refinement, the volume-weighted average crystallite size amounts to 3 nm, which is confirmed by electron microscopy investigations. Figure 1b provides a representative TEM overview image of the TiN nanoparticles. Taking the high temperature of the transformation reaction into account, the TiN nanoparticles are only slightly agglomerated. The TiN particles are quite uniform in morphology. The shape is nearly spherical, and the diameter of the individual nanoparticles is approximately 3 nm (Figure 1b, inset upper right). The nanoparticles form agglomerates with diameters of about 50 nm that are embedded in a matrix of amorphous carbon. Selected area electron diffraction of such an agglomerate exhibits Debye−Scherrer diffraction rings that can be indexed according to cubic TiN and that are typical of a polycrystalline powder (Figure 1b, inset lower left). There are no additional rings or spots in the SAED pattern stemming from any crystalline impurities. The crystallinity is further confirmed by HRTEM investigations. The HRTEM micrograph shows well-developed lattice fringes, which are randomly oriented with respect to each other (Figure 1c), confirming the SAED results. However, the corresponding power spectrum displayed in the inset of Figure 1c indicates, with respect to crystallinity, a two-component character of the TiN sample. The array of discrete spots corresponds to crystalline TiN nanoparticles (the 111 and 200 reflections are denoted), whereas the diffuse superimposed halo can be assigned to amorphous carbon.

The transformation of vanadium oxide to vanadium nitride offers the possibility to investigate the influence of the particle morphology of the starting oxide onto the final shape of the nitride. Two different vanadium oxides were studied as vanadium nitride precursors. V_2O_3 is characterized by an isotropic crystallite shape with diameters in the range of 20−50 nm.[65] The second starting component exhibits an anisotropic, rodlike particle morphology with diameters of about 25−50 nm and lengths between 150 and 250 nm.[64] Both oxides were reacted with cyanamide or urea at 800 °C under a nitrogen atmosphere. Whereas in the case of V_2O_3 only cyanamide was able to transform the oxide completely into the nitride, the vanadium oxide nanorods completely reacted to VN with cyanamide as well as with urea. This observation is rather surprising, as the vanadium oxide nanorods are considerably larger than the V_2O_3 nanoparticles. Obviously, the reactivity of the nanorods toward the nitrogen sources is much higher.

Figure 2 summarizes the structural and morphological features of the various vanadium nitride samples. The powder XRD pattern of VN synthesized from the vanadium oxide nanorods and cyanamide in Figure 2a proves the high crystallinity. All reflections can be assigned to VN (ICDD PDF 35-768) without any indication of other crystalline impurities. According to Rietveld refinement, the volume-weighted average crystallite size amounts to 10.3 nm. The difference profile proves the good quality of fit. The

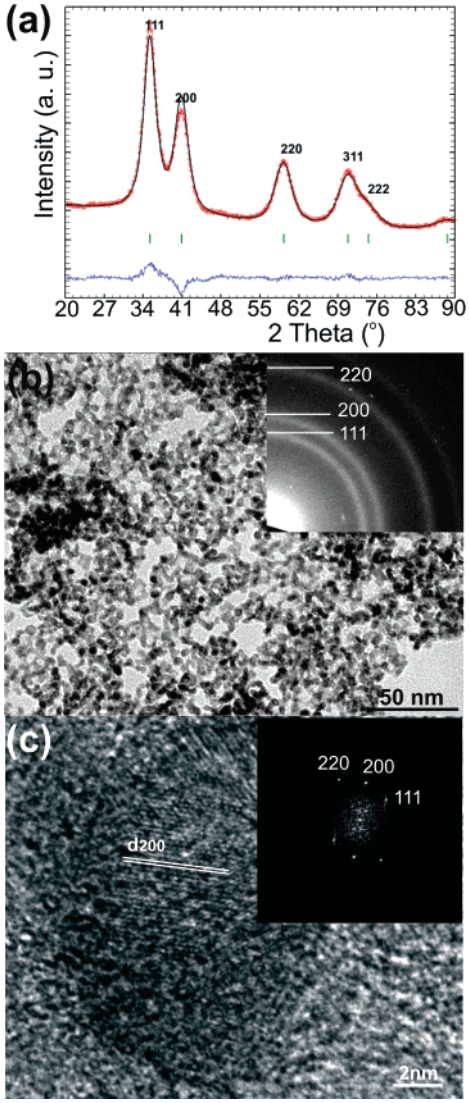

Figure 3. Tantalum nitride nanoparticles obtained from amorphous tantalum oxide and cyanamide. (a) Experimental XRD pattern (red), calculated pattern (black), difference curve (blue), and calculated values of the positions of the Bragg reflections (short green vertical bars). (b) TEM overview image, inset: corresponding SAED pattern. (c) HRTEM image together with the corresponding power spectrum as inset and the lattice indexing.

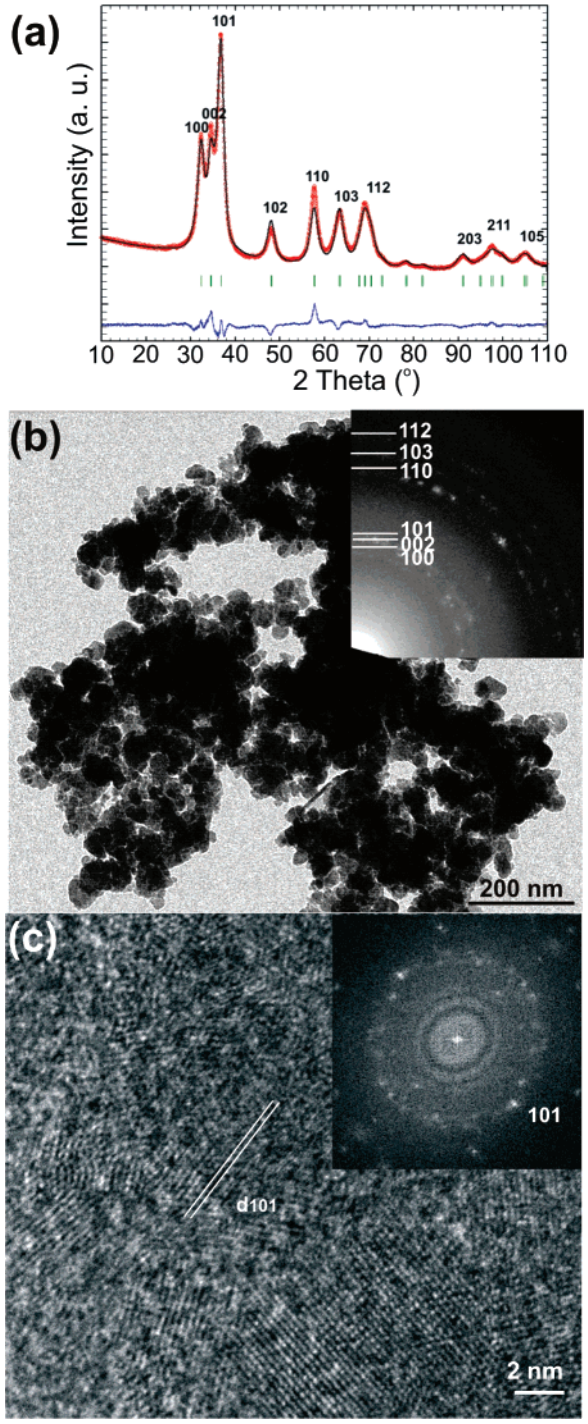

Figure 4. Experimental XRD pattern (red), calculated pattern (black), and difference curve (blue) of GaN. The green short vertical bars represent the calculated values of the positions of the Bragg reflections (ICDD PDF 2-1078). (b) TEM overview image of GaN nanoparticles (inset: corresponding SAED pattern). (c) HRTEM image of GaN with the corresponding PS as inset and the lattice indexing.

crystallite size extracted from the XRD data is confirmed by TEM investigations. Figure 2b displays nanoparticles with sizes in the range of 8−15 nm. The VN nanoparticles obtained from the vanadium oxide nanorods with urea are considerably smaller. The TEM image in Figure 2c shows relatively uniform, nearly spherical particles with diameters of 5−10 nm. The well-developed lattice fringes observed in the HRTEM micrograph (Figure 2c, inset) confirm the high crystallinity. Although in these two cases the VN nanoparticles were obtained from an anisotropically shaped precursor, the morphology of the final product is spherical. The shape of the precursor particles is obviously not transferred to the final nanomaterials. If VN is prepared from V_2O_3 as precursor and cyanamide, the particle size is much larger than in the other two cases. The TEM image in Figure 2d depicts particles in the size range of 20−30 nm. The larger size of the VN nanoparticles prepared from the smaller precursor is presumably due to a dissolution−recrystallization mechanism, in which smaller precursor particles dissolve faster and lead to the recrystallization of larger particles. Also, VN elemental analysis gave evidence for a carbon content of 15−25 wt % for all samples.

The transformation of tantalum oxides into nitrides was investigated mainly with respect to the role of the crystallinity of the precursor materials. Amorphous as well as nanocrystalline tantalum oxide were reacted with cyanamide or urea at 900 °C. In comparison to the other nitrides discussed above, tantalum oxides required a higher reaction tempera-

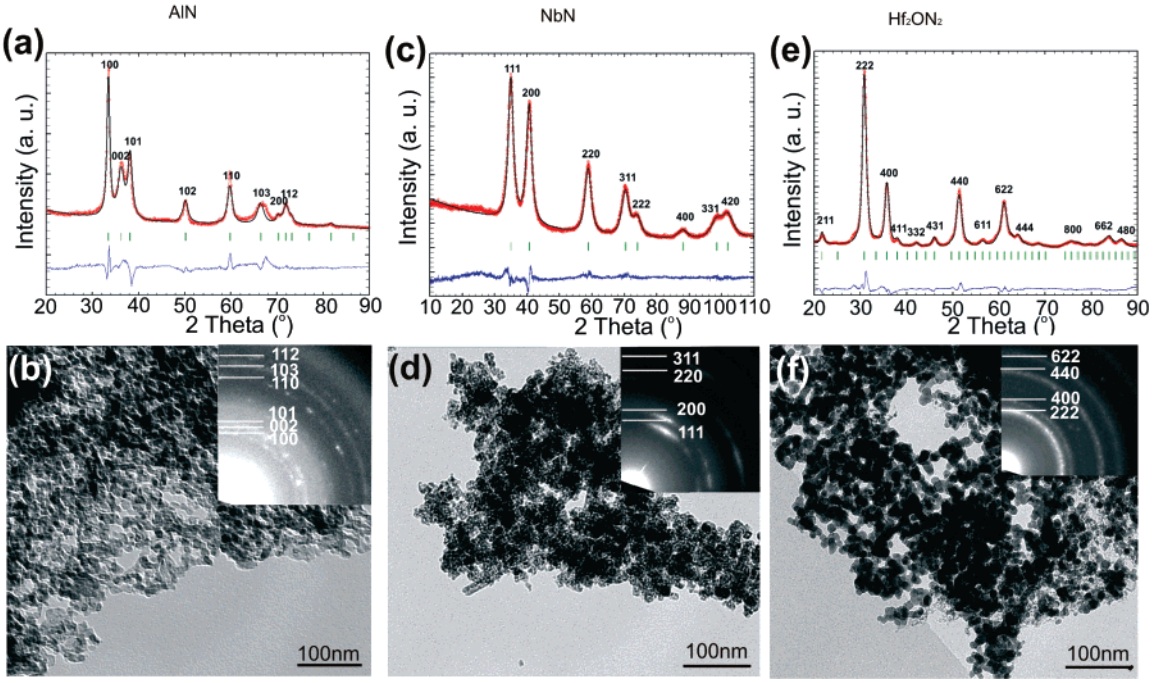

Figure 5. Experimental XRD pattern (red), calculated pattern (black), and difference curve (blue) of (a) AlN, (c) NbN, and (e) Hf_2ON_2, respectively. The green short vertical bars represent the calculated values of the positions of the Bragg reflections. TEM overview images with the corresponding SAED patterns as inset of (b) AlN, (d) NbN, and (f) Hf_2ON_2, respectively.

ture, and in contrast to all the other metal oxides, only amorphous tantalum oxide could be completely converted into tantalum nitride. In the following, TaN nanoparticles prepared from amorphous tantalum oxide and cyanamide are presented. The powder XRD pattern in Figure 3a together with the Rietveld refinement illustrates the high crystallinity of the TaN sample. All reflections correspond to $Fm\bar{3}m$ space group TaN (ICDD PDF 32-1283). The broadness of the peaks points to a small crystallite size, which is confirmed by Rietveld calculations that give a volume-weighted average crystallite size of 2.8 nm. The TEM overview image in Figure 3b displays nanoparticles that are rather uniform in size and shape. They are nearly spherical with diameters ranging from 1.7 to 6 nm. It seems as if there is no amorphous carbon present in the sample, which is confirmed by elemental analysis. The SAED pattern (Figure 3b, inset) shows Debye−Scherrer diffraction rings typical for a polycrystalline powder. The rings can be assigned to the characteristic reflections (111), (200), and (220) of cubic TaN. The crystallinity is further confirmed by HRTEM investigations. Figure 3c shows well-developed lattice fringes. In addition to the crystallinity, the type of nitrogen source is important in the case of TaN. Whereas cyanamide is able to transform the amorphous tantalum oxide completely into TaN, the product obtained in the presence of urea still contained oxidic residues.

The gallium oxide nanoparticles were obtained from gallium acetylacetonate in either benzyl amine,[62] octylamine, or a mixture of both solvents. The crystallite shape of the γ-Ga_2O_3 is nearly spherical, and the average crystallite size calculated from the XRD pattern by Scherrer equation varies from 2 nm (benzylamine) to 2.7 nm (benzylamine/octylamine) and 3.5 nm (octylamine). The gallium oxide nanoparticles are reacted with cyanamide or urea, similar to titania, at 800 °C under nitrogen. In the range of accessible crystallite sizes, all γ-Ga_2O_3 samples were completely transformed into GaN.

In the following, the conversion of 3.5 nm sized γ-Ga_2O_3 in urea is discussed as representative example. Figure 4 displays the experimental X-ray diffraction pattern of GaN together with the calculated pattern obtained from Rietveld refinement and the difference profile. The reflections can be indexed according to the hexagonal phase of GaN (ICDD PDF 2-1078). No other crystalline byproducts were found in the pattern, indicating that the as-prepared sample was pure GaN. The structural parameters from the Rietveld profile refinement are presented in Table 1 in the Supporting Information. The volume-weighted average crystallite size was calculated as 3.9 nm. Anisotropy in line broadening was not observed, so that the crystallite size is expected to be spherical. The extracted values of lattice parameters for the GaN nanoparticles are $a = 3.197$ Å, $b = 3.197$ Å, $c = 5.198$ Å. These values agree well with those obtained from the reported ICDD values for bulk GaN.

The morphological characteristics of GaN were investigated by TEM. A representative overview image in Figure 4b illustrates that the sample consists of nanosized GaN particles. Taking the reaction temperature of 800 °C into account, it is not surprising that the nanoparticles are agglomerated. The grain boundaries are not clearly distinguishable, so that the diameter of the nanoparticles cannot be really determined. The HRTEM micrograph in Figure 4c presents lattice fringes that prove the crystallinity of the sample.

The three GaN samples obtained from the γ-Ga_2O_3 nanopowders with average crystallite sizes of 2, 2.7, and 3.5 nm showed no significant difference in particle morphology. However, the crystallite sizes of GaN calculated from the

101 reflection by the Scherrer equation amounted to about 6, 5, and 4 nm. Similar to VN, the smallest gallium oxide nanocrystallites lead to the formation of the largest GaN crystallites. This observation once again points to a dissolution−recrystallization mechanism. Similar to tantalum nitride but in contrast to all the other metal nitrides, GaN does not contain any carbon impurities, as determined from elemental analysis.

Other metal oxides like aluminum, niobium, and hafnium oxide nanoparticles are also suitable precursors for the preparation of the respective metal nitrides. Figure 5 provides an overview of some other metal oxides that can be transformed to the metal nitrides in the same way. In all these cases, the mixture of oxidic nanopowders with cyanamide or urea was heated to 900 °C to yield the respective metal nitrides. Panels a, c, and e in Figure 5 display the experimental X-ray diffraction patterns of the metal nitrides together with the calculated patterns obtained from Rietveld refinement and the difference profiles. Again, no other crystalline byproducts were found. The structural parameters from the Rietveld profile refinement are presented in Table 1 in the Supporting Information. The reflections can be indexed according to the hexagonal phase of AlN (ICDD PDF 44-106), cubic phase of NbN (ICDD PDF76-263) and cubic phase of Hf_2ON_2 (ICDD PDF 88-669). According to the SAED pattern (inset Figure 5b) the AlN nanoparticles exhibit satisfying crystallinity. The clearly distinguishable grain boundaries make it possible to determine the diameter of the nanoparticles to 5−10 nm, which agrees well with the Rietveld refinement data. In the case of NbN, the crystallite size extracted from the XRD pattern (Figure 5c) is about 4 nm. The strongly agglomerated particles on the TEM image in Figure 5d do not allow a reasonable determination of the particle size. The SAED pattern (inset in Figure 5d) shows the characteristic (111) reflection of cubic NbN at 0.256 nm, in addition to the (200), (220), and (311) reflections. The experimental and calculated XRD patterns of Hf_2ON_2 in Figure 5e provide a volume-weighted average grain size of 7 nm, which is in good agreement with the particle size observable on the TEM image in Figure 5f. The high crystallinity of the powder leads to well-pronounced Debye−Scherrer diffraction rings in the SAED pattern (Figure 5f, inset) that can be assigned to the reflections (222), (400), (440), and (622).

Conclusions

The thermal transformation of metal oxide nanoparticles into metal nitrides was investigated with the focus on finding a correlation between the morphological and structural characteristics of the starting oxide nanoparticles with the final metal nitrides. Metal oxide nanoparticles with different particle sizes, shapes, and degree of crystallinity were reacted with cyanamide or urea as nitrogen sources. However, general conclusions are difficult to draw because of the different reactivities of the various metal oxides toward the two nitrogen sources. For example, in the case of titania, the upper crystallite size for complete transformation from the oxide to the nitride is less than 10 nm, whereas in the case of vanadium oxide, nanorods with sizes up to hundreds of nanometers react readily to the respective nitride. The degree of crystallinity seems to play a minor role for most of the metal oxides investigated. However, tantalum oxide reacts only to the metal nitride, if an amorphous nanopowder is used as starting material. Although GaN and TaN do not show any indication for carbon impurities, all the other metal nitrides contain carbon in the range of 15−25 wt %. In none of the investigated cases was the morphology of the oxidic compound transferred to the metal nitride, which means that the reaction pathway presumably proceeds along a dissolution−recrystallization process. Independent of the crystallite sizes of the oxidic precursor particles that can be as large as 250 nm in the case of the VO_x nanorods, all the obtained metal nitrides are in the size range of 3−20 nm, generally with a rather small size distribution. Although the size and the shape of the starting oxidic nanomaterials are not retained during the thermal transformation, they still do influence the morphology of the final metal nitride nanoparticles. Together with the nitrogen source, the variation of the morphological and structural characteristics of the metal oxide nanoparticles provide a precious tool to control the size of the metal nitride nanocrystals to some extent.

Acknowledgment. We thank the Max Planck Society for the financial support.

Supporting Information Available: Detailed experimental procedures; structural results and refinement parameters obtained from Rietveld analysis of the experimental XRD powder data of all samples; EDX analysis of TiN, VN, and GaN. This material is available free of charge via the Internet at http://pubs.acs.org.

CM0701759